ARMA 18–265

# Application of Micromechanical Modeling to Prediction of In-Situ Rock Behavior

Sinha, S.
*Colorado School of Mines, Golden, Colorado, United States*
Walton, G.
*Colorado School of Mines, Golden, Colorado, United States*



This paper was prepared for presentation at the 52nd US Rock Mechanics / Geomechanics Symposium held in Seattle, Washington, USA, 17–20 June 2018. This paper was selected for presentation at the symposium by an ARMA Technical Program Committee based on a technical and critical review of the paper by a minimum of two technical reviewers. The material, as presented, does not necessarily reflect any position of ARMA, its officers, or members. Electronic reproduction, distribution, or storage of any part of this paper for commercial purposes without the written consent of ARMA is prohibited. Permission to reproduce in print is restricted to an abstract of not more than 200 words; illustrations may not be copied. The abstract must contain conspicuous acknowledgement of where and by whom the paper was presented.

**ABSTRACT:** With advances in numerical modeling techniques, Voronoi Tessellations are being increasingly used to generate simulated grain structures for investigation of small-scale damage processes in rocks. In a Voronoi model, a material is represented as an aggregate of polygonal blocks that interact through contacting interfaces. Typically, a set of input micro-parameters is calibrated to numerically replicate the macroscopic mechanical behavior of the rock under study. The calibration is mostly restricted to attributes estimated from laboratory testing, such as damage threshold levels, uniaxial compressive strength and tensile strength. While the potential of Voronoi Tessellations in modeling small-scale damage processes has been extensively tested, its utility in capturing field-scale behavior is largely unexplored. This study attempts to bridge the gap through development of a calibrated laboratory scale model of Creighton granite followed by upscaling it to an 8 m wide pillar. An assessment of the Voronoi model's abilities and shortcomings were investigated through a qualitative and quantitative comparison of the model's macroscopic behavior against empirically validated continuum model results recently published by the authors and documented pillar behaviors as seen in the field.

## 1. INTRODUCTION

In recent years, the Discrete Element Method (DEM) has been increasingly used for the study of micromechanical damage processes in intact rocks. The development of this approach was driven by the inability of continuum models to explicitly simulate fracture opening and separation – a mechanism by which damage localizes primarily along grain contact boundaries. In addition, continuum model results are heavily dependent on the choice of a constitutive relationship.

In DEM models of intact rock, the material is represented by an aggregate of circular or polygonal blocks that can interact through the contacting interfaces. The calculation procedure oscillates between Newton's law of motion and a force-displacement contact law, eliminating the need to assign a macroscopic material constitutive model. The macroscopic behavior of the simulated model depends on the choice of micro-parameters. Specifically, the micro-parameters can be classified into two groups: (a) Block properties, and, (b) Contact properties. The combined effect of both sets of parameters control the emergent macroscopic behavior of the model.

The formal pioneers of this modeling approach are Diederichs (1999) and Potyondy and Cundall (2004), who developed the Bonded Particle Method (BPM). In BPM, a material is simulated using circular disks/sphere that can interact through parallel contact bonds. Although novel and structurally homologous to rock mineral assemblages, it suffers from some limitations, such as inability to simultaneously match the material compressive and tensile strength, a linear failure envelope, low friction angles and reduced tendency of incipient fractures to propagate (Diederichs, 1999; Potyondy and Cundall, 2004). Subsequent developments like cluster particle models (Potyondy and Cundall, 2004), the flat-joint model (Potyondy, 2012) and clumped particle models (Cho et al., 2007) were able to partially overcome some of the limitations associated with the traditional BPM. The main issue, however, remains the high inherent porosity and lack of particle interlocking due to the circular/spherical shape of constituent blocks.

The Voronoi tessellation represents an improvement over conventional BPM and utilizes triangular/polygonal blocks to characterize the material domain. As a result, particle interlocking issues are avoided. In terms of the mechanistic difference between polygonal and triangular blocks (also called trigons), it was pointed out by several authors (e.g. Ghazvinian et al., 2014; Mayer and Stead, 2017) that models with triangular elements have a predisposition towards shear failure due to the availability of potential linear failure pathways. Laboratory tests of rocks have shown damage to initiate in a tensile mode at about 25-40% of the uniaxial compressive strength (Diederichs, 2007). As a result, polygonal Voronoi blocks

are better suited for studying the deformation and failure mechanisms in intact crystalline rocks.

The current study is focused on assessing the capabilities of the Voronoi tessellation approach in simulating the damage processes in field-scale engineering structures in rock. To that end, a small-scale synthetic model of Creighton granite was developed, with parameters calibrated against the Uniaxial Compressive Strength (UCS), Brazilian Tensile strength (BTS), Crack Damage Threshold (CD) and Crack Initiation Threshold (CI). An additional check for model consistency was accomplished through a comparison of the evolution of dilation angle against those measured in laboratory, which is the first such comparison known to the authors. With its abilities examined, the small-scale model was subsequently enlarged to correspond to an 8 m wide pillar with W/H varying from 1-3. The overall behavior of these pillar models was compared against recently developed and empirically verified continuum models results (Sinha and Walton, 2018) and documented pillar behaviors as observed in the field (Krauland and Soder, 1987).

Several authors have attempted to capture the behavior of large scale structures using DEM. Garza-Cruz et al. (2014) used a 3-dimensional tetrahedral grain-based model to study the stability of tunnels in brittle rocks. Coggan et al. (2012) and Gao and Stead (2014) used a similar technique to investigate the roadway stability in coal mines. Christianson et al. (2006) performed triaxial tests on a 1m x 1m lithophysal tuff sample with varying degree of porosity for aiding the design of a nuclear waste repository at Yucca Mountain, Nevada. Azocar (2016) attempted to replicate the brittle fracture processes observed in the URL Mine-by Experiment test tunnel through a comparative analysis of tetrahedral and polygonal block models. Interestingly, most of the previously studies that successfully replicated field-scale behaviors have utilized tetrahedral/ triangular blocks even though they tend to underestimate the degree of tensile damage.

Upscaling a laboratory size model to a field-scale structure is cumbersome and computationally challenging if the block size is to be kept unchanged. Most studies in past have used a larger element size, although a good understanding of the effect of block size on the emergent model behavior is not fully understood. For this study, the block size was increased by 40 times (~2.5 mm to ~10 cm) when transitioning from the lab scale to the pillar scale (10 cm longest dimension to 8 m longest dimension) to obtain an acceptable runtime for the pillar models. As will be later shown in this paper, the block size exerts a major influence on the model results, often overshadowing the effect of micro-parameters. Very low block-contact strength properties were required to obtain stress-strain curves comparable to those expected.

In addition to the biases involving selection of a constitutive relationship, continuum models also tend to underestimate the ground-support interaction effect (Sinha and Walton, 2017). As discussed by Sinha and Walton (2017), the root cause is the inability of such models to allow separation of failed boundary elements, thereby implicitly accounting for the effect of supports that act primarily as a strain-boundary for damaged material. In contrast, DEM softwares possess the capability of block detachment as fractures develop and coalesce in the model. A rib bolt, under such circumstances, would function more efficiently by limiting the bulking of rockmass. Clearly, a DEM approach is more effective in assessing support needs over conventional continuum approaches.

## 2. DEM SIMULATION OF CREIGHTON GRANITE

### *2.1. Laboratory data*

The granitic rock selected for this study is from the Main Orebody at Creighton Mine, located at the southern edge of the Sudbury Igneous Complex (SIC) in Canada (Walton, 2014). The rock was geomechanically characterized by Walton (2014) on the basis of laboratory tests, and the relevant properties are listed in Table 1. The authors would like to point out that the granite in the mine is fairly massive, meaning the laboratory derived intact properties can be considered representative of the overall rockmass (Kaiser et al., 2000; Carter et al., 2008; Walton et al., 2016).

In-situ brittle failure initiates at a stress level corresponding to the Crack Initiation Threshold (CI) observed in laboratory tests (Martin, 1997; Diederichs, 2007). Given that this study has the ultimate goal of modeling mine pillars, where failure initiates through surficial spalling, CI was chosen as a key calibration parameter. Away from the excavation boundary, the dilation-induced confinement suppresses the formation of tensile cracks, causing the failure mode to transition from tension to shear. The Crack Damage (CD) Threshold represents the long-term laboratory shear strength and it was also considered as a point of calibration. With no CD values for the Creighton Granite reported by Walton (2014) or Walton et al. (2016), a calibration target for CD corresponding to 80-90% of the mean UCS was selected.

Table 1. Geomechanical properties of Creighton Granite.

| Parameter | Value |
|---|---|
| Uniaxial Compressive Strength (UCS) | 200 MPa |
| Young's Modulus | 52 GPa |
| Poisson's Ratio | 0.1 |
| CI (unconfined) | 85 MPa |
| Brazilian Tensile Strength (BTS) | 10.5 MPa |

To further constrain the calibration process, a representative stress-strain curve was developed through

mathematical averaging of 20 individual stress-strain curves. The following steps, in sequence, were followed: (1) First, each of the 20 curves was normalized such that the peak stress occurred at (1, 1); (2) The average peak strength (i.e. UCS) and the axial strain corresponding to the peak strength was computed; (3) The normalized axial strain range (0-1.1) was subdivided into 220 bins and the stresses within each bin were averaged to generate the average normalized curve (see black line in Fig 1a); (4) The normalized curve was rescaled back such that the peak occurred at the stress and strain levels computed in step 2; (5) The initial non-linear portion of the curve, corresponding to crack closure, was replaced by a linear section (red dashed line in Figure 1b) and translated to the left such that the corrected curve commenced from (0,0). The removal of the non-linear section was necessary because Voronoi models represent zero porosity systems with no pre-existing cracks. Figure 1 illustrates the methodology followed for obtaining the averaged laboratory stress-strain curve.

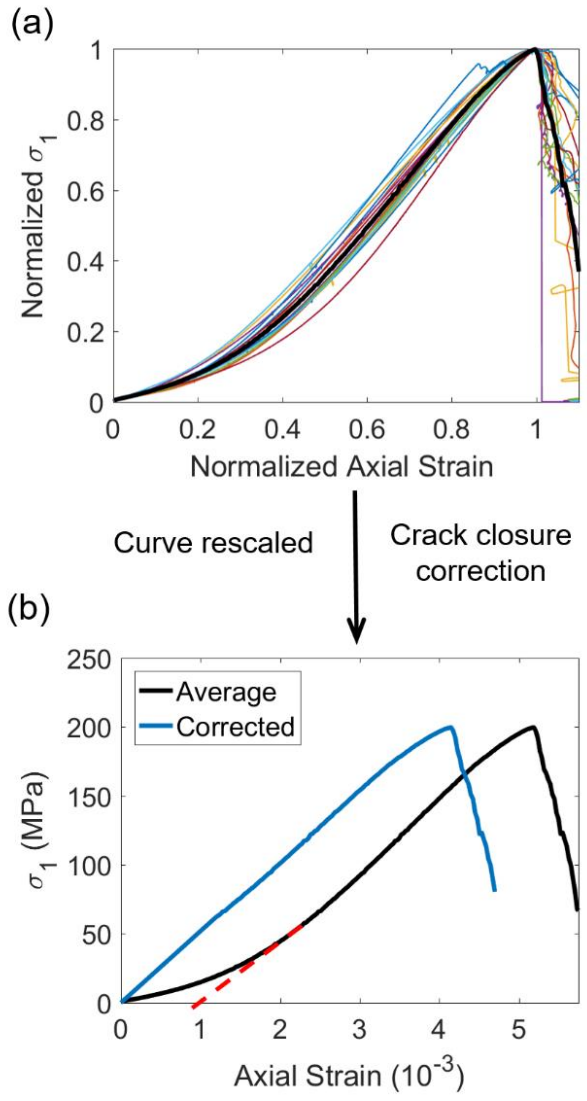


Figure 1. Methodology for obtaining a representative stress-strain curve for Creighton granite from 20 individual curves.

### *2.2. Numerical Modeling: Specimen Generation, Calibration and Results*

The applicability of Voronoi Tessellation for simulation of brittle micro-fracturing in crystallize rocks was tested through a series of UCS and Brazilian tests in the explicit DEM software UDEC. Explicit numerical softwares rely on a time-march algorithm that assumes a limited speed for transmission of disturbances within a material (Jing and Stephansson, 2007). Details of the mathematical equations and their implementation are beyond the scope of this paper and can be found in Jing and Stephansson (2007).

For the UCS test, a cylindrical (rectangular in two dimensions) 55 mm x 120 mm specimen with 2.5 mm blocks was selected (Figure 2). The block size is consistent with what has been previously used for modeling granitic rocks (Kazerani and Zhao, 2010; Nicksiar and Martin, 2014). The sample was loaded from the top using a servo-controlled velocity boundary condition. The built-in servo function modifies the applied velocity as a function of the unbalanced forces in the model. The upper bound of the velocity was set at 0.005 m/sec (Fabjan et al., 2015). The steady post-peak portion of the laboratory stress-strain curves implied that the loading system was very stiff; as a result, the platens were omitted to simulate an infinitely stiff loading mechanism.

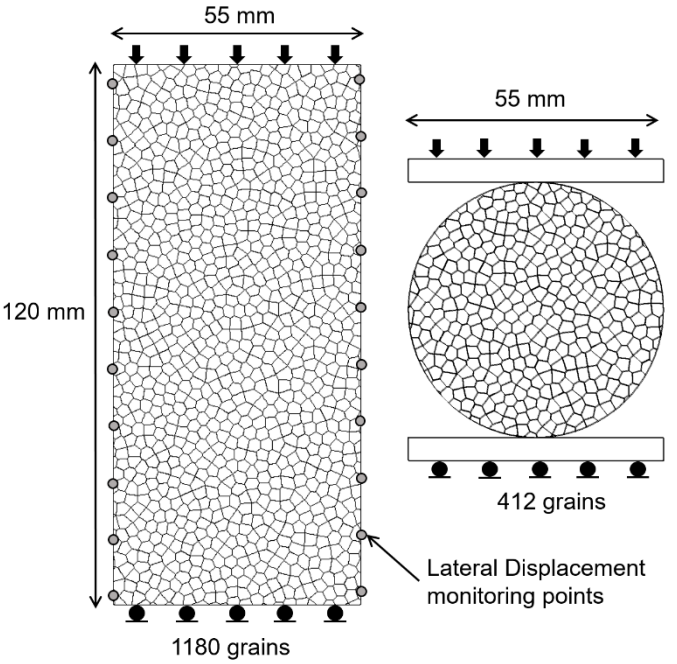


Figure 2. Geometric setup of the UCS and the Brazilian test model.

The Brazilian sample was a circular disc with 55 mm diameter, loaded through two platens on either side. The block size and the loading mechanism are similar to the UCS model. Figure 2 shows the geometry of the UCS and the Brazilian models. For the UCS model, the axial stress was computed every 1000 solution steps by dividing the

cumulative reaction force at the top surface by the width of the model. A similar methodology was used for computing the stresses in the BTS model.

Axial and lateral strains were also computed for the UCS model as the difference in displacement along two opposite edges divided by the distance between them. While every gridpoint on the top and bottom surface were used for axial strain calculation, only 10 monitoring points on either edge of the model were utilized for computing the lateral strains (see Figure 2). This reduced the simulation time drastically. In case of the BTS model, the total reaction force was converted to tensile stress using the equation:

$$\sigma_t = \frac{2P}{\pi D t} \qquad \text{(Eq. 1)}$$

Where P is the total reaction force, D and t are the specimen diameter and width, respectively.

The CI and CD thresholds can be identified as the points of non-linearity in the lateral and axial stress-strain curve, respectively (Lajtai, 1974; Diederichs and Martin, 2010; Nicksiar and Martin, 2012). A simpler approach, however, is to track the development of tensile and shear fractures in UDEC models. The stress level corresponding to the initiation of tensile fracturing can be designated as CI (Nicksiar and Martin, 2014) while the point where the shear crack accumulate begins to accelerate represents the CD (Farahmand and Diederichs, 2015). CD can also be identified as the point of reversal in the axial strain-volumetric strain curve (Diederichs and Martin, 2010).

While it may be simpler to just track the number of tensile and shear fractures using built-in FISH variables, users must take note of the fact that tensile fractures can transition to shear fractures and vice-versa, as the model equilibrates towards a quasi-static solution. It is therefore necessary to track the evolution of fractures in addition to their aggregate number in the models. A comparison using the UCS model revealed that the number of tensile fractures could be underestimated by as much as 20% near the peak strength when simply using built-in FISH variables to track aggregate numbers of different crack types.

The contact and block micro-parameters were modified to match the macro-properties listed in Table 1, following the procedure suggested by Ghazvinian et al. (2014):

(1) The Young's Modulus (E) and Poisson's ratio (ν) of blocks were selected according to the macroscopic E and ν of Creighton granite.

(2) The contact normal to shear stiffness ratio controls the macroscopic Poisson's ratio. Therefore, kn/ks was varied until the desired Poisson's ratio was obtained.

(3) The normal stiffness (kn) was adjusted to match the Young's modulus.

(4) With the elastic parameters constrained, the contact tensile strength was adjusted to match the CI threshold.

(5) Finally, different combinations of contact cohesion and friction angle were tested to match the Brazilian tensile strength, CD threshold and peak strength. The calibrated set of input parameters and the resulting macro-properties are listed in Table 2.

Table 2. Contact micro-parameters and model-predicted macroproperties.

| Parameters | Value |
|---|---|
| *Contact Input Properties* | |
| Contact cohesion (peak) - $c_{peak}$ | 100 MPa |
| Contact cohesion (residual) - $c_{res}$ | 0 MPa |
| Contact friction angle (peak) - $\phi_{peak}$ | 0º |
| Contact friction angle (residual) - $\phi_{res}$ | 47º |
| Dilation angle - $\psi$ | 5º |
| Contact tensile strength - $\sigma_t$ | 18 MPa |
| Normal Stiffness ($k_n$) | 23000 GPa/m/m |
| Shear Stiffness ($k_s$) | 16000 GPa/m/m |
| *Emergent Macroscopic Properties* | |
| Uniaxial Compressive Strength (UCS) | 201 MPa |
| Young's Modulus | 52.1 GPa |
| Poisson's Ratio | 0.12 |
| CI (unconfined) | 85 MPa |
| CD (unconfined) | 185 MPa |
| Brazilian Tensile Strength | 10.3 MPa |

Figure 3a shows the stress-strain curve obtained from the Voronoi model. A striking resemblance in both the pre-peak and post-peak response could be observed when compared to the average laboratory curve. The CI, CD and the tensile strength are also consistent with previously reported laboratory test results for Creighton Granite.

To assess the model's ability in capturing the lateral dilational behavior, volumetric strain was computed using the equation:

$$\varepsilon_v = \varepsilon_y + 2\varepsilon_x \qquad \text{(Eq. 2)}$$

Where, $\varepsilon_y$ is the axial strain, and, $\varepsilon_x$ is the lateral strain. Upon plotting the volumetric strain versus the axial strain (see Figure 3b), the CD threshold appears to coincide fairly well with the point of stress-reversal as expected for a crystalline rock under unconfined conditions (Martin, 1997; Diederichs & Martin, 2010; Ghazvinian, 2010). Further analysis on the model's macroscopic dilatational behavior is presented in the next section.

The fracture pattern in the UCS model is shown in Figure 3b while the tensile stress-strain curve and the fracture pattern for the BTS model is shown in Figure 4. The UCS model fails via tensile splitting along the left edge and some form of macro-shear (through coalescence of tensile fractures) along the right edge. These observations conforms closely with what was observed in the laboratory UCS samples post-testing. In the BTS model, a through-going fracture was identified that terminated at the two opposite platens.

### 2.3. *Dilatancy of the Voronoi Model*

Dilatancy is the volumetric expansion of a yielding rock or rockmass. It is strongly related to the post-yield stress-strain response of laboratory specimens. At the excavation scale, it controls bulking and the interaction of support with the rockmass. With respect to the ultimate goal of investigating the behavior of large-scale structures, it crucial to assess the model's potential to exhibit a realistic dilatant behavior.

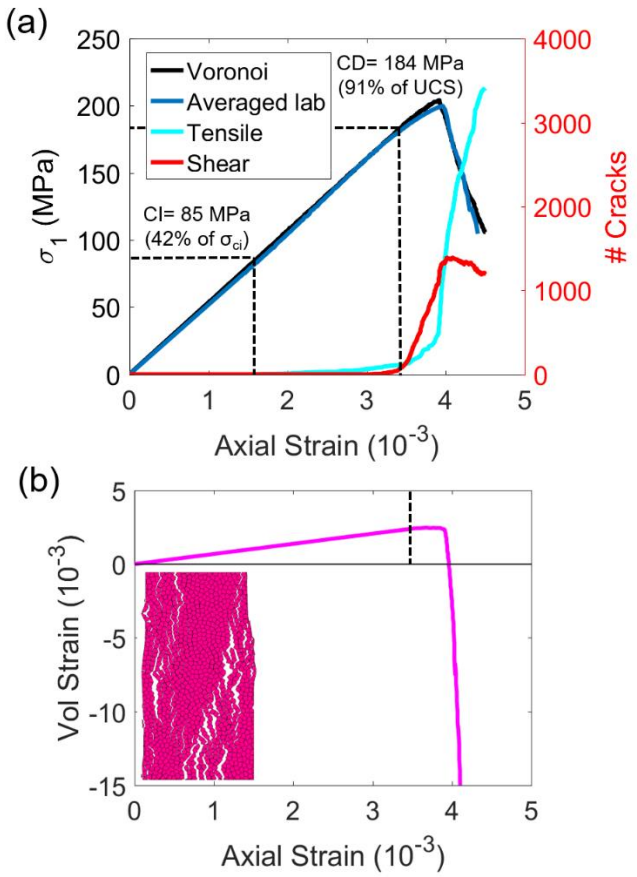


Figure 3. (a) Stress-strain curve and other damage thresholds for Voronoi UCS; (b) Volumetric vs axial strain.

The macroscopic dilatancy of a specimen can be quantified using the parameter, dilation angle ($\psi$), which relates the maximum ($\dot{\epsilon}_1^p$) and minimum ($\dot{\epsilon}_3^p$) principal inelastic strain increments (see Eq. 3). Several studies have found the dilation angle to be a function of confining stress ($\sigma_3$) and plastic shear stain ($\gamma^p$) (Alejano and Alonso, 2005; Zhao and Cai, 2010; Walton and Diederichs, 2015). Since only UCS tests have been simulated here, only the plastic shear strain dependency of the dilation angle will be considered. The plastic shear strain is a variable that quantifies system damage and can be computed from internal variables using Eq. 4.

$$\sin(\psi) = \frac{\dot{\varepsilon}_v^p}{-2\dot{\varepsilon}_1^p + \dot{\varepsilon}_v^p} \quad \text{(Eq. 3)}$$

$$\gamma^p = \varepsilon_1^p - \varepsilon_3^p \quad \text{(Eq. 4)}$$

The inelastic principal strains were calculated following the methodology proposed by Walton et al. (2014) and Walton and Diederichs (2015), which utilizes the elasticity theory and accepted definitions of CI and CD (Diederichs and Martin, 2010). A brief discussion of the approach and associated equations (Eq. 5-7) are presented below.

When calculating the maximum and minimum plastic strains using Equation 5s and 6, the middle terms represent a correction to ensure zero plastic axial strain at CD and zero plastic lateral strain at CI, in accordance with the definitions of CI and CD per Diederichs and Martin (2010). The last term signifies the elastic component that must be subtracted to obtain the respective plastic strain values. Once obtained, the plastic volumetric strains are computed using Eq. 7. It is noted here that the lateral strain in the laboratory was measured using a chain along the center of the sample. In contrast, the lateral strain in the model was monitored at 20 locations along the edge, which could yield slightly different results.

$$\varepsilon_1^p = \varepsilon_1 - \varepsilon_{1\,(CD)} - \frac{\sigma_1 - CD}{E} \quad \text{(Eq. 5)}$$

$$\varepsilon_3^p = \varepsilon_3 - \varepsilon_{3(CI)} - \nu\frac{\sigma_1 - CI}{E} \quad \text{(Eq. 6)}$$

$$\varepsilon_v^p = \varepsilon_1^p + 2\varepsilon_3^p \quad \text{(Eq. 7)}$$

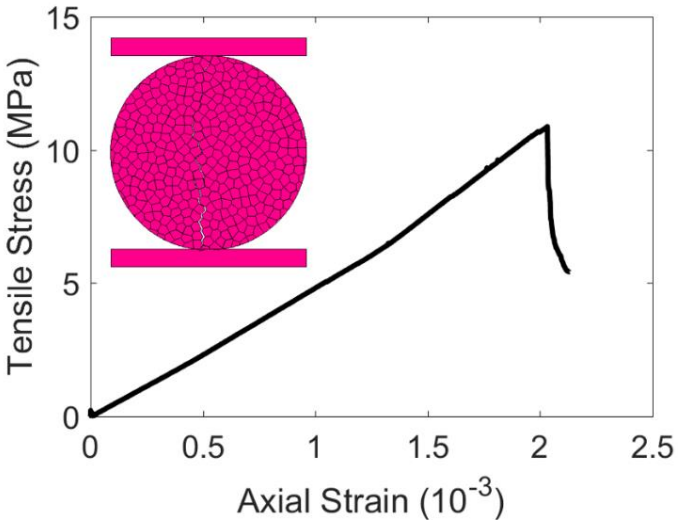


Figure 4. Tensile stress-strain curve with fracture pattern for the BTS model.

To provide a basis for comparison between the Voronoi model results and the laboratory data, median, upper bound and lower bound dilation angle models (Walton & Diederichs, 2015) to dilation data from individual UCS tests were developed. These three results (shown by bold black and green lines in Figure 5a) were utilized in testing the model's ability of reproducing a realistic dilatant behavior. As can be seen from Figure 5b, the model-predicted instantaneous dilation angles are well within the upper and lower bounds of the laboratory data. The dilation model parameters for the laboratory median fit

and the fit to the dilation angle values extracted from the Voronoi model (see Figure 5b) are listed in Table 3.

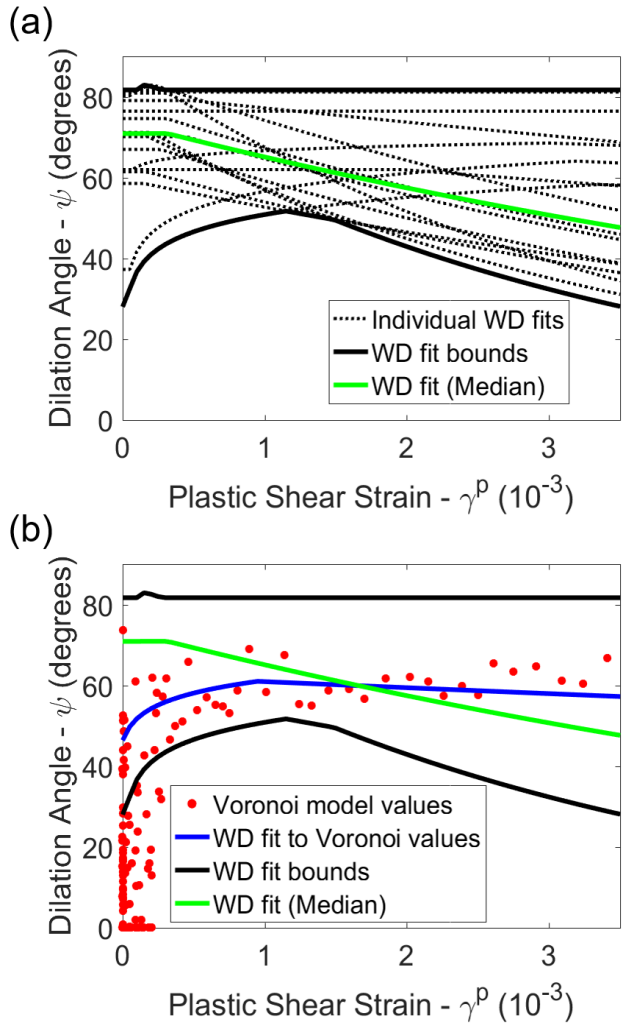


Figure 5. (a) Walton & Diederichs (2015) dilation angle models (termed "WD") obtained from laboratory UCS tests of Creighton Granite with the median fit and fit bounds indicated; (b) dilation angle values extracted from the Voronoi UCS model versus plastic shear strain compared to dilation angle trends in the laboratory.

Table 3. Walton & Diederichs (2015) dilation angle model (termed "WD") fit parameters.

| **Parameter and Influence** | **Median Laboratory WD Fit** | **Voronoi WD Fit** |
|---|---|---|
| $\alpha$ – Pre-Mobilization curvature | 0 | 0.08 |
| $\gamma_m$ – Plastic shear strain at peak $\psi$ | 0.0003 | 0.001 |
| $\gamma^*$ – Decay Rate | 0.008 | 0.02 |
| $\Psi_{peak}$ – Peak dilation angle | 70° | 64° |

While the fit to the Voronoi model dilation angle values appropriately characterizes the overall trend in the dataset, the pre-mobilization curvature parameter is substantially higher than the laboratory median fit. The cause for this discrepancy is not immediately evident and requires further study. Additionally, the decay in the post-mobilization portion of the curve was also found to be smaller, and could be related to the different lateral strain measurement scheme or the model's inability to replicate shearing of asperities. Despite these minor discrepancies between the modeled dilation behavior and that observed from laboratory testing, the small-scale Voronoi model was able to reproduce the overall trends in the dilation angle observed in laboratory UCS tests.

## 3. PILLAR MODELS

With the micro-parameters constrained against laboratory derived attributes, the next logical step was to upscale the model to simulate an 8 m wide pillar. A key issue when attempting to model large structures using Voronoi is the selection of an appropriate block size. Since using the same block size as in the small-scale Voronoi models would be computationally restrictive, 0.1 m Voronoi blocks were utilized. Three separate models were developed, corresponding to W/H of 1, 2 and 3. The overall geometry and loading mechanism (elastic beam on either side) was chosen to correspond to the continuum pillar models of Sinha and Walton (2018). Figure 6 shows the geometry for W/H=1 pillar model.

It is known that Voronoi model outputs are dependent on the block size chosen (Ghazvinian et al., 2014; Fabjan et al., 2015; Insana et al., 2016). Use of the micro-parameters constrained against small-scale attributes resulted in excessively high peak strengths for the pillar models. To obtain micro-parameters which resulted in reasonable macroscopic pillar behavior, the pillar models were calibrated against the stress-strain responses obtained from the continuum (FLAC$^{3D}$) pillar models.

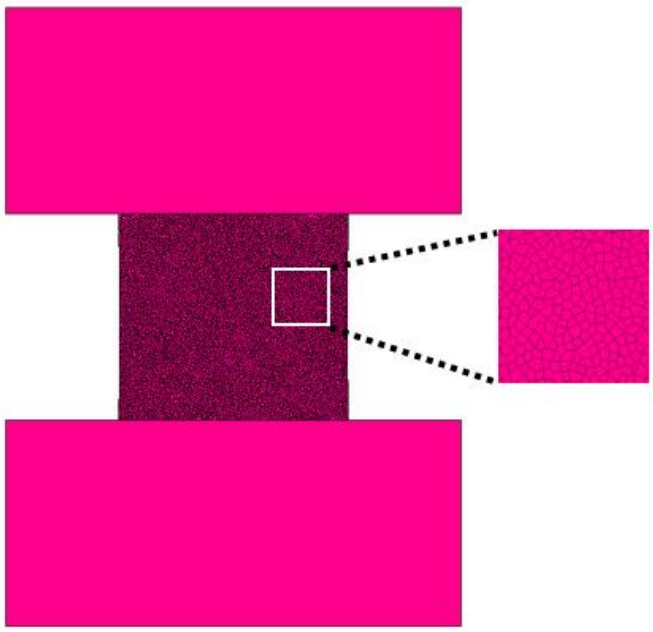

Figure 6. Voronoi pillar model setup (W/H=1).

Sinha and Walton (2017) explained how continuum models implicitly account for the presence of support acting as a strain boundary to prevent the gradual degradation of pillars due to loss of spalled material. Calibrating the Voronoi micro-parameters against the continuum model results, without any modification, would therefore be inappropriate.

To mimic the pillar degradation associated with the loss of spalled material at the edges of pillars, the authors developed a 'deletion' code whereby all boundary elements in the FLAC$^{3D}$ pillar models under tension and exceeding a pre-defined plastic shear strain limit (damage level associated with spalling) were incrementally deleted as the model was loaded through a constant downward velocity. FLAC$^{3D}$ models calibrated to in-situ pillar strength observations for supported pillars were re-run using the 'deletion' code; the resulting stress-strain curves from these sets of models were considered more appropriate for direct comparison with the UDEC models, which explicitly allow for the separation of spalled material from the pillars.

Figure 7 compares the stress-strain curves from FLAC$^{3D}$ with those obtained in UDEC after model calibration. The associated micro-parameters are also listed in Table 4. Although these calibrated curves match quite well, the three UDEC model calibrations required independent parameter input sets, meaning that the micro-parameters used are not fundamental to the material being modeled. Specifically, very low friction angle and high peak cohesion for the contacts was necessary to replicate the brittle behavior of W/H=1 pillar. On the other hand, a higher friction angle and lower peak cohesion was required to initiate faster yield and continued pre-peak hardening. As a consequence of the model's inability to predict expected pillar strengths using a single set of parameters, it is believed that use of homogenous elastic Voronoi blocks maybe too simplistic to capture the complete range of expected pillar behavior.

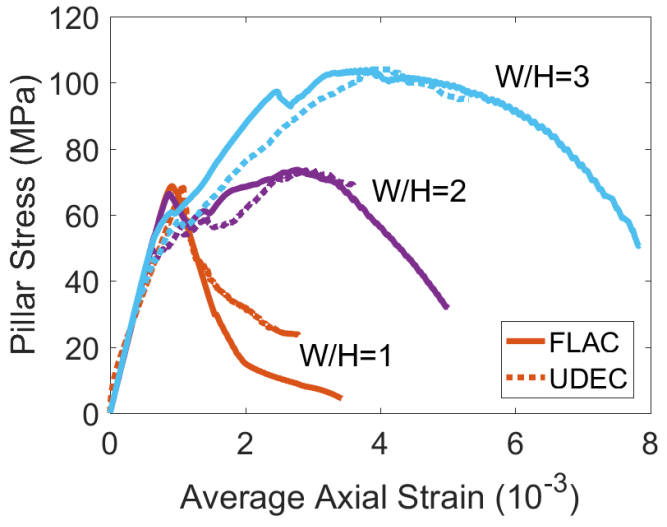


Figure 7. Stress-strain curves from UDEC and FLAC$^{3D}$.

Figure 8 shows the major principal stress contour for W/H=3 pillar model at peak strength. The hourglassing phenomenon, exhibited by the highly stressed core, is an evidence of the progressive damage mechanism typically associated with pillars. In the W/H=1 model, no confined core was generated since the failure was due to the formation of a cross-shear plane (refer Figure 9; the plot was generated at a strain of 0.0015). The spalling and bulking of the rib was found to be more pronounced in the W/H=3 model, although some corner failures was seen in the W/H=1 model. The macro-failure mechanism changes from brittle to ductile with W/H=2 acting as the transition point (refer to the pre-peak hardening in the stress-strain response for W/H=2 model).

Table 4. Contact micro-parameters for different W/H models.

| Parameters | Values | | |
|---|---|---|---|
| | W/H=1 | W/H=2 | W/H=3 |
| $c_{peak}$ (MPa) | 135 | 60 | 50 |
| $c_{res}$ (MPa) | 0 | 0 | 0 |
| $\phi_{peak}$ | 0º | 0º | 0º |
| $\phi_{res}$ | 5º | 21º | 17º |
| $\Psi$ | 5º | 5º | 5º |
| $\sigma_t$ (MPa) | 10 | 10 | 10 |
| $k_n$ (GPa/m/m) | 23000 | 23000 | 23000 |
| $k_s$ (GPa/m/m) | 16000 | 16000 | 16000 |

Despite the inability of Voronoi to capture the entire range of pillar behavior using a single set of micro-parameters, each of the calibrated models themselves can be used for a variety of purposes (e.g. support effect testing), as long as they demonstrate the basic pillar failure mechanisms and reproduce realistic stress-strain response. This is a major advantage over conventional continuum models that implicitly account for the effect of skin support. Use of a discontinuum modeling approach is therefore critical to a successful pillar support design (bolts and/or mesh).

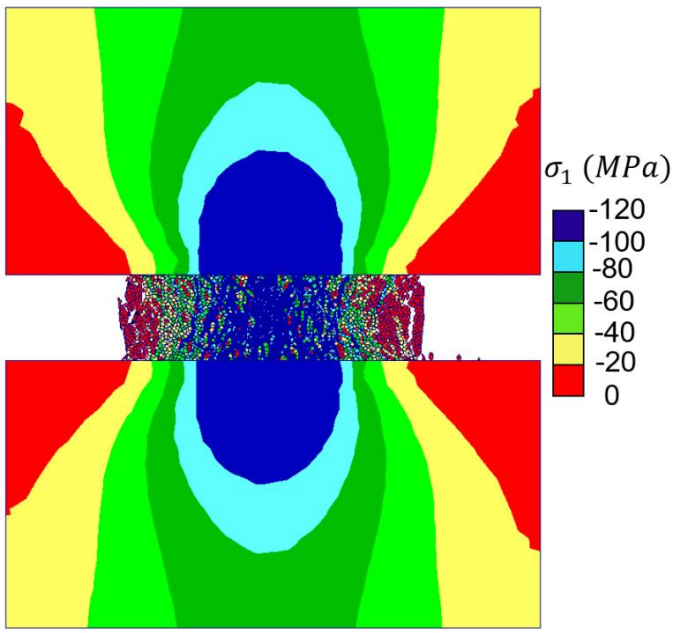


Figure 8. Major principal stress contour for W/H=3 model.

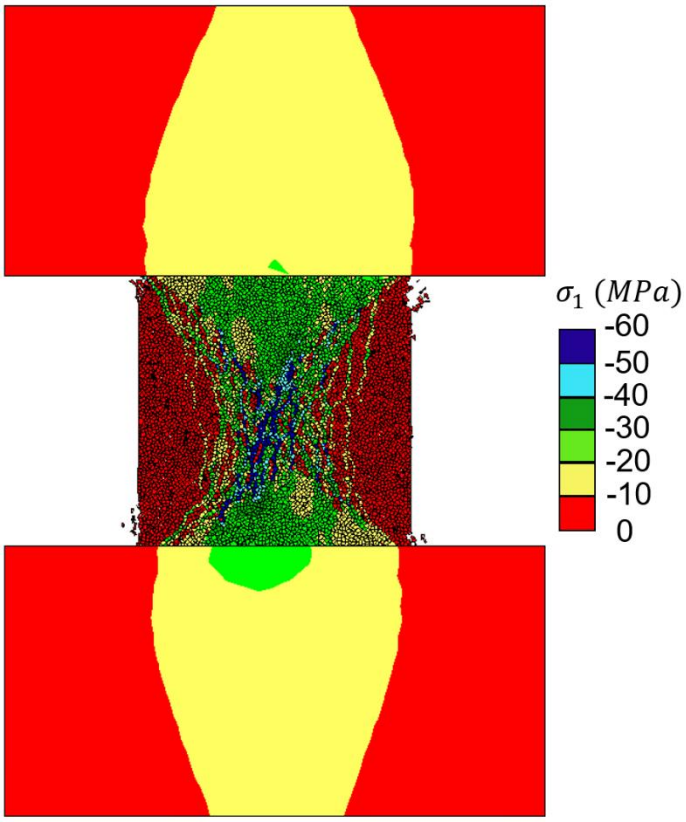


Figure 9. Major principal stress contour for W/H=1 model in its post-peak portion.

## 4.0 CONCLUSIONS

While the Voronoi Tessellation approach has been found to be effective in simulating small-scale damage processes in brittle crystalline rocks, its ability in modeling field-scale structures is still largely unexplored. This study was performed with a focus on assessing the abilities and shortcomings of Voronoi in simulating large underground structures, like mine pillars.

To that end, a synthetic small-scale model of Creighton granite was generated, with micro-parameters constrained against laboratory-derived attributes (UCS, BTS, CI and CD). Additionally, the overall pre- and post-peak stress-strain curves and the macroscopic dilatational behavior exhibited by the model were consistent with laboratory data. The model was subsequently enlarged to simulate three 8 m wide pillars with W/H of 1, 2 and 3. Because Voronoi model results are dependent on the block size selected, the contact properties had to be recalibrated. The average stress-strain response from continuum pillar models, recently developed by the authors, was used for this purpose.

A single set of micro-parameters was found to inadequate in capturing the range of behavior that is expected from slender (brittle) and squatter (semi-ductile to ductile) pillars. This suggests that approach of using homogeneous, elastic Voronoi blocks does not allow for the fundamental mechanics of field-scale damage processes to be captured. Additionally, this work serves as a cautionary tale that an impressive laboratory-scale model calibration does not ensure that the modeling approach used (let alone the specific parameters selected) can be universally applied, let alone used for predictive purposes.

## ACKNOWLEDGEMENT

The research conducted for this study was funded by the National Institute of Occupational Health and Science (NIOSH) under Grant Number 200-2016-90154. The authors would like to extend their sincere gratitude for this financial support. The authors would also like to thank Mark Christianson from Itasca for his valuable inputs and troubleshooting assistance.

## REFERENCES

1. Alejano, L.R. and A., Alonso. 2005. Consideration of dilatancy angle in rock and rock masses. *Int J Rock Mech Min Sci*, 42:481-507.
2. Azocar, K. 2016. *Investigating the mesh dependency and upscaling of 3D grain-based models for the simulation of brittle fracture processes in low porosity crystalline rock.* M.A.Sc Thesis, Queen's University, Ontario, Canada.
3. Carter, T.G., M.S., Diederichs and J.L., Carvalho. 2008. Application of modified Hoek-Brown transition relationships for assessing strength and post-yield behavior at both ends of the rock competence scale. Procs *6th International Symposium on Ground Support in Mining and Civil Engineering Construction*, Cape Town, South Africa.
4. Cho, N., C.D., Martin and D.C., Sego. 2007. A clumped particle model for rock. *International Journal of Rock Mechanics and Mining Sciences*, 44(7):997-1010.
5. Christianson, M., M. Board and D., Rigby. 2006. UDEC simulation of triaxial testing of lithophysal tuff. Procs 41st *U.S. Rock Mechanics/Geomechanics Symposium*, Golden, Colorado.
6. Coggan, J., F.Q., Gao, D., Stead and D., Elmo. 2012. Numerical modelling of the effects of weak immediate roof lithology on coal mine roadway stability. *International Journal of Coal Geology*, 90-91(1): 100-109.
7. Diederichs, M.S. 1999. *Instability of hard rockmasses: The role of tensile damage and relaxation*. PhD Thesis. University of Waterloo, Ontario, Canada.
8. Diederichs, M.S. 2007. The 2003 geotechnical colloquium: Mechanistic interpretation and practical application of damage and spalling prediction criteria for deep tunnelling. *Canadian Geotechnical Journal*, 44:1082-1116.
9. Diederichs, M.S. and C.D., Martin. 2010. Measurement of spalling parameters from laboratory testing. *In Zhao, Labiouse, Dudt & Mathier (Eds.), Rock mechanics in civil and environmental engineering*. London: Taylor & Francis Group.
10. Fabjan, T., D.M., Ivars and V., Vukadin. 2015. Numerical simulation of intact rock behavior via continuum and Voronoi tessellation models – A sensitivity analysis. *Acta Geotechnica Slovenica*, 5-23.

11. Farahmand, K. and M.S. Diederichs. 2015. A calibrated Synthetic Rock Mass (SRM) model for simulating crack growth in granitic rock considering grain scale heterogeneity of polycrystalline rock. Procs *49th U.S. Rock Mechanics/Geomechanics Symposium*, San Francisco, CA.
12. Gao, F.Q. and D., Stead. 2014. The application of a modified Voronoi logic to brittle fracture modelling at the laboratory and field scale. *International Journal of Rock Mechanics and Mining Sciences*, 86:1-14.
13. Garza-Cruz, T.V. and M.E., Pierce. 2014. A 3DEC Model for heavily veined massive rock masses. Procs *48th U.S. Rock Mechanics/Geomechanics Symposium*, Minneapolis, Minnesota.
14. Ghazvinian, E. 2010. *Modelling and testing strategies for brittle fracture simulation in crystalline rock samples.* M.A.Sc Thesis, Queen's University, Ontario, Canada.
15. Ghazvinian, E., M.S., Diederichs and R., Quey. 2014. 3D random Voronoi grain-based models for simulation of brittle rock damage and fabric-guided micro-fracturing. *Journal of Rock Mechanics and Geotechnical Engineering*, 6(6): 506-521.
16. Insana, A., M., Marla and D., Elmo. 2016. Multiscale numerical modelling related to hydrofracking for deep geothermal energy exploration. *Procedia Engineering*, 158:314-319.
17. Jing, L and O., Stephansson. 2007. *Fundamental of Discrete Element Methods for Rock Engineering: theory and application*. Elsevier, Amsterdam, Netherland.
18. Kaiser, P.K., M.S., Diederichs, C.D., Martin, J., Sharp and W., Steiner. 2000. Underground works in hard rock tunneling and mining. Procs *Geoeng 2000*, Melbourne, Australia.
19. Kazerani, T. and J., Zhao. 2010. Micromechanical parameters in bonded particle method for modeling of brittle failure. *International Journal for Numerical and Analytical Methods in Geomechanics*, 34(8): 1877-1895.
20. Krauland, N. and P.E., Soder. 1987. Determining pillar strength from pillar failure observation. *Engineering Mining J.*, 8:34-40.
21. Lajtai. EZ. 1974. Brittle fracture in compression. *International Journal of Fracture Mechanics*, 10:525-536
22. Martin, C.D. 1997. Seventeenth Canadian geotechnical colloquium: The effect of cohesion loss and stress path on brittle rock strength. *Canadian Geotechnical Journal*, 34:698-725.
23. Mayer, J.M. and D., Stead. 2017. Exploration into the causes of uncertainty in UDEC Grain Boundary Models. *Computer and Geotechnics*, 82: 110-123.
24. Nicksiar, M. and C.D., Martin. 2012. Evaluation of methods for determining Crack Initiation in compression tests on low-porosity rocks. *Rock Mechanics and Rock Engineering*, 45(4): 607-617.
25. Nicksiar, M. and C.D., Martin. 2014. Factors affecting crack initiation in low porosity crystalline rocks. *Rock Mechanics and Rock Engineering*, 47(4): 1165-1181.
26. Potyondy, D.O. and P.A., Cundall. 2004. A bonded-particle model for rock. *International Journal of Rock Mechanics and Mining Sciences*, 41(8): 1329-1364.
27. Potyondy, D.O. 2012. A flat-jointed bonded-particle material for hard rock. Procs *46th U.S. Rock Mechanics/Geomechanics Symposium*, Chicago, Illinois.
28. Sinha, S. and G., Walton. 2017. Modeling the effect of bolts on the behavior of rock pillars and associated insights on rib reinforcement". Procs 36th *International Conference on Ground Control in Mining*, Morgantown, West Virginia.
29. Sinha, S., and G., Walton. 2018. Development of a Progressive S-Shaped Yield Criterion and its application to the study of rock pillar behavior. *International Journal of Rock Mechanics and Mining Sciences* (Resubmitted).
30. Walton, G. 2014. *Improving continuum models for excavations in rock masses under high stress through an enhanced understanding of post-yield dilatancy.* Ph.D. Thesis. Queen's University, Kingston, Canada, 2014.
31. Walton, G., M.S., Diederichs and J., Arzua. 2014. A detailed look at pre-peak dilatancy in a granite-determining "plastic" strains from laboratory test data. Procs *Eurock 2014*, Vigo, Spain.
32. Walton, G. and M.S. Diederichs. 2015. A new model for the dilation of brittle rocks based on laboratory compression test data with separate treatment of dilatancy mobilization and decay. *Geotechnical and Geological Engineering*, DOI:10.1007/s10706-015-9849-9.
33. Walton, G., M.S., Diederichs and A. Punkkinen. 2015. The influence of constitutive model selection on predicted stresses and yield in deep mine pillars-A case study at the Creighton mine, Sudbury, Canada. *Geomechanics and Tunneling*, 5:441-449.
34. Walton, G., M.S., Diederichs, A., Punkkinen and J., Whitmore. 2016. Back analysis of a pillar monitoring experiment at 2.4 km depth in the Sudbury basin, Canada. *International Journal of Rock Mechanics and Mining Sciences*, 85:33-51.
35. Zhao, X.G. and M., Cai. 2010. A mobilized dilation angle model for rocks. *International Journal of Rock Mechanics and Mining Sciences*, 47:368-384.